

Gas and dust properties in the afterglow spectra of GRB 050730

R. L. C. Starling¹, P. M. Vreeswijk², S. L. Ellison³, E. Rol⁴, K. Wiersema¹, A. J. Levan^{4,5}, N. R. Tanvir⁵, R. A. M. J. Wijers¹, C. Tadhunter⁶, J. R. Zaurin⁶ & R. M. Gonzalez Delgado⁷.

¹ Astronomical Institute 'Anton Pannekoek', University of Amsterdam, Kruislaan 403, 1098 SJ Amsterdam, The Netherlands.
e-mail: starling@science.uva.nl

² European Southern Observatory, Alonso de Córdova 3107, Casilla 19001, Santiago 19, Chile.

³ Dept. of Physics and Astronomy, University of Victoria, Elliott Building, 3800 Finnerty Rd, Victoria, BC, V8P 1A1, Canada.

⁴ Dept. of Physics and Astronomy, University of Leicester, University Road, Leicester LE1 7RH, UK.

⁵ Dept. of Physical Sciences, University of Hertfordshire, College Lane, Hatfield, Herts. AL10 9AB, UK.

⁶ Dept. of Physics and Astronomy, The Hicks Building, University of Sheffield, Sheffield S3 7RH, UK.

⁷ Instituto de Astrofísica de Andalucía (CSIC), PO Box 3004, 18080 Granada, Spain.

Received ; accepted

Abstract. We present WHT ISIS optical spectroscopy of the afterglow of gamma-ray burst GRB 050730. The spectrum shows a DLA system with the highest measured hydrogen column to date: $N(\text{H I}) = 22.1 \pm 0.1$ at the third-highest GRB redshift $z = 3.968$. Our analysis of the *Swift* XRT X-ray observations of the early afterglow show X-ray flares accompanied by decreasing X-ray absorption. From both the optical and the X-ray spectra we constrain the dust and gas properties of the host galaxy. We find the host to be a low metallicity galaxy, with low dust content. Much of the X-ray absorbing gas is situated close to the GRB, whilst the H I absorption causing the DLA is most likely located further out.

Key words. gamma rays: bursts - galaxies: distances and redshifts - cosmology: observations

1. Introduction

Gamma-ray bursts (GRBs) have proven to be excellent probes of the distant Universe. The high luminosities of GRB afterglows allow absorption line studies of the ISM at high redshift to at least $z = 4.5$ (see Andersen et al. 2000). The launch and successful operation of the *Swift* satellite means more GRBs are being localised and afterglows studied. Subsequently, the number of high redshift bursts suitable for host galaxy spectral studies has dramatically increased. Deep observations of afterglow positions have detected host galaxies in almost all cases (e.g. Conselice et al. 2005). Most hosts are compact, low-metallicity, actively star-forming galaxies and are found to have low intrinsic extinction. However, in a few cases, radio / submm observations of hosts give a star-formation rate (SFR) which is of order a few to ~ 100 larger than rates derived from optical estimators such as the line luminosities of $\text{H}\alpha$ and $[\text{O II}]$ or the 2800 Å restframe UV continuum flux (e.g. Berger et al. 2003). This may be caused by strong dust obscuration, but neither spectra nor colours of hosts show strong internal extinction. Afterglow spectroscopy provides a unique window on the near environment of GRBs (see e.g. GRB 021004), allowing us to probe the absorbing dust and gas properties in more detail. In this Letter we present optical and X-ray spectra of GRB 050730, discovered by *Swift* on July 30th 2005, 19:58:23

UT (Holland et al. 2005) and lying at a redshift of $z = 3.97$ (Chen et al. 2005; Rol et al. 2005), in which we study the circumburst gas and dust properties.

2. The optical afterglow spectra

2.1. Observations

During the afterglow phase of GRB 050730, we acquired spectra using the Intermediate-dispersion Spectroscopic and Imaging System (ISIS) on the William Herschel Telescope. The R316R and R300B grisms were used on the red and blue arms respectively. Two observations were done sequentially, with exposure times of 1260 and 1800 seconds. The first observation started at 22:57 UT at airmass ~ 2.73 (midpoint 0.132 days after burst), the second at 23:19 UT (midpoint 0.145 d) and airmass ~ 3.4 . The seeing quality at the high airmasses required the slit width to be widened to 2.5 arcsec. Both spectra have been reduced using the data reduction package IRAF following standard procedures. A Galactic extinction correction of $E(B-V) = 0.049$ (Schlegel et al. 1998) was applied. The wavelength resolutions of blue- and red-arm spectra respectively are 8.7 and 8.1 Å. The signal to noise per pixel, measured at 6800 Å, is 27 in the first spectrum and 17 in the second spectrum.

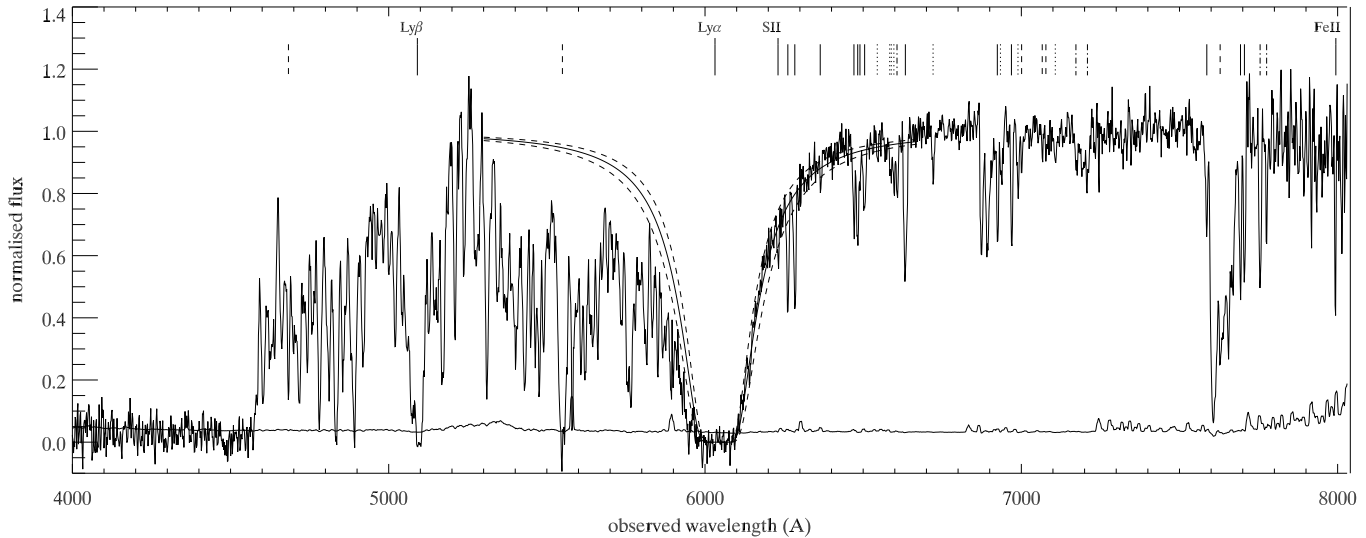


Fig. 1. The WHT ISIS combined, normalised spectrum of the afterglow (midpoint 0.14 days), and 1σ error spectrum (lower curve). Overlaid is the best-fitting DLA profile (solid line) and its errors (dashed lines). All significant lines (3σ) are indicated above for $z = 3.969$ (solid), $z = 3.565$ (dashed), $z = 1.773$ (dot-dashed) and unidentified (dotted) systems; see on-line table for details. Lines used in further analysis are labelled.

2.2. Results

The spectrum is rich in line features at $z = 3.97, 3.56$ and 1.77 (e.g. Prochaska et al. 2005). A strong Damped Lyman-Alpha absorption system (DLA) is present; here we focus on this and a selection of metal lines in the GRB host galaxy. We fitted a power law continuum corrected for Galactic extinction to the ~ 6500 – 7500 Å region of each spectrum, excluding the absorption lines. We investigated whether this red part of the spectrum showed any departure from a pure power law due to host-galaxy extinction, but fitting of MW, LMC and SMC extinction curves (Pei 1992) shows the extinction to be consistent with zero. Conditions during the observations were not photometric, so we have normalised and combined the spectra, shown in Fig. 1. The optical/IR spectral slope may also be obtained by fitting the photometric points. We did this using published B , V , R , I and J band data extrapolated to a common epoch, adopting a temporal decay index of 0.89 (Haislip et al. 2005; Holman et al. 2005; Cobb et al. 2005; Blustin et al. 2005), and find $\beta \sim -1$, consistent with that measured from continuum fits to our optical spectra. However, there are currently insufficient photometric data available for a quantitative analysis.

Despite the moderate dispersion of the ISIS 300 grisms, the damping wings of the host galaxy DLA are clearly visible. In fact, the determination of $N(\text{HI})$ in DLAs based on long slit spectra is considerably simpler than for echelles. Since the damped profile may extend over many spectral orders in a typical echelle, accurate combination and flux calibration can be troublesome. Using the Starlink software DIPSO, we determine $\log N(\text{HI}) = 22.1 \pm 0.1$ (1σ); our fit is shown in Fig. 1. Taking $\text{Ly}\beta$ into account did not lead to a more accurate determination of $N(\text{HI})$, and the error on our fit is dominated by extrapolation of the power law continuum across the $\text{Ly}\alpha$ forest. The $N(\text{HI})$ value is consistent with, although slightly lower than, that reported by Prochaska et al. (2005). This high value

(the first DLA to break the 10^{22} atoms cm^{-2} barrier) continues the trend amongst GRBs towards very high neutral hydrogen columns (e.g. Vreeswijk et al. 2004).

Although our spectra do not enable as detailed a study of the metal lines as is possible via echelle observations, we briefly comment on a selection of the metals lines detected in our spectrum. Detection limits are quoted at the 3σ level. Based on the detection of $\text{S II } \lambda 1253$ with a restframe equivalent width $\text{EW} = 0.29 \pm 0.05$ Å, and assuming that this line is not saturated, we determine $\log N(\text{S II}) = 15.3$. Combined with the $N(\text{HI})$ value and a solar S abundance of $\log (\text{S/H}) + 12 = 7.20$ (Grevesse & Sauval 1998), this gives $[\text{S/H}] = -2.02$. Although the low EW indicates that the $\text{S II } \lambda 1253$ transition is not heavily saturated, we cannot rule out mild saturation which would make the calculated abundance a lower limit. We determine an upper limit of $[\text{S/H}] < -1.99$ based on the absence of the weaker $\text{S II } \lambda 1250$ line in our spectrum. Similarly, from the $\text{Fe II } \lambda 1608$ line which is partially saturated and the undetected $\text{Fe II } \lambda 1611$, we determine $-2.92 < [\text{Fe/H}] < -1.92$. A search for variability in line features between our two spectra, separated by ~ 25 mins, revealed no significant changes (see on-line table for details), neither did the $N(\text{HI})$ column vary.

3. The absorbed X-ray afterglow

3.1. Observations

We have analysed the early *Swift* XRT data, to look for evidence of intrinsic absorption in the X-ray spectrum. The XRT data consist of Windowed Timing (WT) mode data for the first orbit (133 to 793 seconds after the trigger) and start of the second orbit, and Photon Counting (PC) mode data for later orbits. The data were reduced using the standard pipeline for XRT data within the HEADAS 6.0 package (*Swift* software version 2.0). WT mode data was extracted using a rectangular region

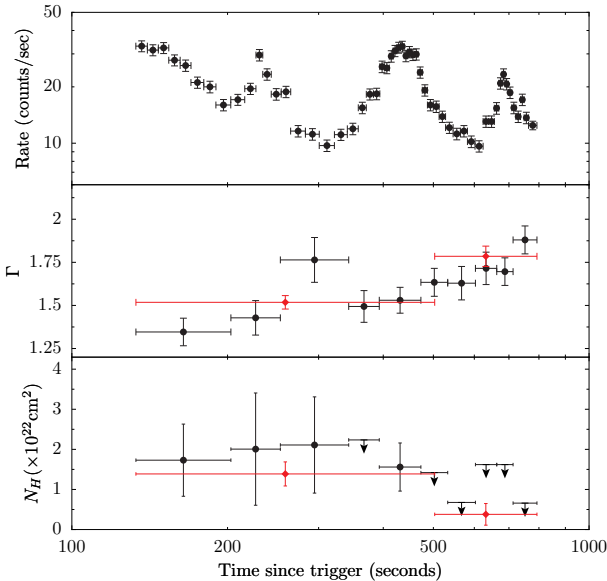


Fig. 2. Evolution of the 0.3–10 keV count rate (top), absorbing column, N_H , 0.2–10 keV power law slope, Γ (middle) and additional equivalent hydrogen column, $N_{H,\text{int}}$, at the redshift of the host galaxy (bottom) during the first ~ 800 s of the *Swift* XRT observations (90% errors). Filled circles show the values for the individual spectra; the two combined spectra pre- and post 500 s, for which better constraints are obtained, are shown with diamonds.

centred on the source, and a similar area in a source-free region of the same image to determine the background level. PC mode data was extracted using a circular aperture, except for orbits 2 to 4 which show evidence of pile-up (count rates $\gtrsim 0.8$ counts s^{-1}) and were extracted using an annular region centred on the source and filtered on grade 0 only. The light curve was obtained between channels 30 and 1000 (spanning ~ 0.3 –10 keV). Spectral analysis was done using XSpec 11.3, with the standard Ancillary Response Function (ARF) files, which estimate the effective telescope area, for PC mode data, and with ARFs based on ray-tracing ('physical' ARFs) for WT mode data which should provide a better calibration at low energies.

3.2. Results

The first orbit shows several flares in the light curve, first reported by Grupe et al. (2005). We have performed a detailed analysis of the spectral evolution of the early-time data. The fitted model consists of a power law plus Galactic absorption (fixed at $3.05 \times 10^{20} \text{ cm}^{-2}$, Dickey & Lockman 1990) and a variable Galactic-like absorption component at $z = 3.97$. Errors are quoted at the 90% confidence level for 1 interesting parameter. We find evidence for a change in power law photon index, from $\Gamma = 1.52 \pm 0.04$ at the start of the first orbit to 1.79 ± 0.06 at the end of the orbit (note that $\Gamma = -(1 + \beta)$). We also find evidence for an excess absorption column, which at the redshift of the burst amounts to an intrinsic column of $N_{H,\text{int}} = (1.4 \pm 0.3) \times 10^{22} \text{ cm}^{-2}$. However, around 500 seconds post trigger, the absorption column abruptly changes, becoming lower by at about

a factor of 4, $N_{H,\text{int}} = (3.4 \pm 2.7) \times 10^{21} \text{ cm}^{-2}$. In the later time PC mode spectrum the intrinsic column cannot be constrained, setting an upper limit of only $N_{H,\text{int}} \leq 1.0 \times 10^{22} \text{ cm}^{-2}$, and the power law photon index remains stable at $\Gamma = 1.77$. We have checked for a possible correlation between the intrinsic $N_{H,\text{int}}$ and Γ in the fit. Contour plots for the interval between 133 and 503 seconds and for the interval between 503 and 793 seconds post trigger show no evidence for any correlation, confirming the reality of both the drop in $N_{H,\text{int}}$ and increase in Γ (Fig. 2). Interestingly, this happens directly after the peak of the second visible flare, where the light curve intensity has increased by a factor of 3. Given the host galaxy metallicity we measure in the optical spectrum, we adjust the X-ray absorption model accordingly. Using $Z = 1/100Z_\odot$ for all the elements heavier than He included in the zvphabs X-ray absorption model, the required intrinsic equivalent hydrogen column increases by a factor of ~ 10 in both cases to $N_{H,\text{int}} = 9.5_{-2.1}^{+2.3} \times 10^{22} \text{ cm}^{-2}$ (first 400 s) and $N_{H,\text{int}} = 2.6_{-1.6}^{+1.9} \times 10^{22} \text{ cm}^{-2}$ (500 s post trigger).

A preliminary analysis of published optical photometry together with the PC mode XRT spectrum has shown the X-ray and optical slopes at 0.19 days ($\beta_X \sim -0.7$ to -0.8 , $\beta_{\text{opt}} \sim -1.0$ to -1.4) to likely be incompatible with a position of the cooling break between the optical and X-rays, and might suggest the presence of an inverse Compton component; we await the availability of further optical/IR photometry for a full analysis.

4. Discussion and conclusions

4.1. Host galaxy properties

There is a well known relationship between galaxy luminosity and metallicity (e.g. Garnett 2002; Lamareille et al. 2004) which spans 6 orders or more of magnitude in M_B . Tremonti et al. (2004) have recently demonstrated that this relation is driven by an underlying relation between mass and metallicity. The cause of the relationship, they argue, is due to the increased gravitational potential of massive galaxies which enhances metal retention. In the absence of a detected host for GRB 050730 at the time of writing, it is in principle possible to use the luminosity-metallicity (LZ) and mass-metallicity (MZ) relations to predict the M_B and stellar mass of the host. Both of these relations are best determined locally (e.g. Lamareille et al. 2004), although sizeable datasets have now investigated the LZ relation up to $z \sim 1$ (e.g. Kobulnicky et al. 2003; Kobulnicky & Kewley 2004). There is clear evidence for evolution in the LZ relation, in the sense that galaxies are more metal-poor for their luminosity at higher z (although see the caveats in Kewley & Ellison in prep.). This trend appears to continue both for the LZ and MZ relations up to $z \sim 3$ (e.g. Shapley et al. 2004; Erb et al. in prep.), although only the highest mass/luminosity galaxies are bright enough to be included in spectroscopic samples. The lowest metallicity bin in the fitted MZ relation of Erb et al. (in prep.) is $Z \sim 1/3 Z_\odot$ corresponding to a stellar mass $\log(M_\star) \sim 9.5 M_\odot$. The metallicity measured from absorption lines in the OA considered here is $Z \sim 1/100 Z_\odot$, which indicates that the host is not a massive, luminous Lyman break galaxy, although Fynbo et al. (2003) argue that GRB hosts follow the same UV luminosity function

as the faint LBGs. We do note that the MZ relation is based on *emission* lines. However, HST imaging has shown that GRBs occur in regions of strongest star formation, justifying our assumption that the absorption lines are formed in the same regions as the higher wavelength emission lines.

Combining the measured $N(\text{HI})$ with the metallicity and assuming an SMC gas-to-reddening ratio (Bouchet et al. 1985), we can estimate the extinction associated with the GRB host galaxy and compare this to the values obtained from the optical continuum fits. Negligible $E(B - V)$ is determined by both methods, consistent with the similarly small amounts of dust seen towards intervening DLAs (e.g. Murphy & Liske 2004; Ellison, Hall & Lira 2005).

We detect no $\text{Ly}\alpha$ emission in the trough, although in the absence of a reliable flux calibration, we cannot put a limit on the star formation rate. Previously, GRB 021004 (Møller et al. 2002), GRB 030323 (Vreeswijk et al. 2004) and possibly GRB 020124 (Hjorth et al. 2003) have all been found to exhibit $\text{Ly}\alpha$ emission super-imposed on the DLA trough. It has been suggested (e.g. Fynbo et al. 2003) that the low metallicity of GRB hosts (required for the collapsar model) may explain the prevalence of $\text{Ly}\alpha$ emission, but the metallicity of GRB 050730's host is a factor of 5 lower than GRB 030323 and has a lower dust content. However, the $N(\text{HI})$ of GRB 050730 is 50% higher than GRB 030323, so there will be more diffusion of $\text{Ly}\alpha$ photons from resonant scatterings. The lack of $\text{Ly}\alpha$ may simply be a geometric effect, i.e. if the $\text{Ly}\alpha$ emitting region simply did not fall on the ISIS slit. Narrow band $\text{Ly}\alpha$ imaging follow-up will be an interesting way to determine if the emission is weaker in this host compared with previous bursts.

4.2. The neutral hydrogen column

GRB 050730 has the strongest DLA seen in a GRB afterglow spectrum, with a hydrogen column density of $\log N(\text{HI}) = 22.1 \pm 0.1$. The X-ray absorption at late times scaled to $Z_\odot/100$ yields a comparable $\log N_{\text{H,int}} = 22.4^{+0.2}_{-0.4}$. The intrinsic absorption is, however, significantly lower at Solar abundance where we find $\log N_{\text{H,int}} = 21.5^{+0.2}_{-0.7}$ (in both cases assuming the $N_{\text{H,int}}$ measured at ~ 500 – 800 s post burst in the WT mode XRT spectrum can be extrapolated to a few hours post burst). It should be noted that what is measured in the X-ray model is an equivalent hydrogen column, since primarily metal edges contribute to the X-ray absorption at the redshift of GRB 050730, meaning that $N_{\text{H,int}}$ is an upper limit to the amount of neutral hydrogen present (see e.g. Wilms et al. 2000).

The intrinsic equivalent hydrogen column measured in the early-time X-ray spectra covering ~ 133 – 500 s post trigger is about ten times higher than that measured at $t > 500$ s. The change in X-ray absorbing column could be caused by ionisation by either the gamma-ray jet or the X-ray flares, which are suggested to be caused by prolonged central engine activity (Burrows et al. 2005; King et al. 2005). A decrease in X-ray absorption has also been linked to the X-ray flare observed in the early afterglow of GRB 050502B (Burrows et al. 2005), where the change in column density is much more pronounced.

The X-ray absorbing gas in GRB 050730 is therefore located close to the GRB. The optical H I column remained stable over the ~ 25 mins between our ISIS spectra, taken at 0.132 days since burst, well after the observed X-ray flaring (although the occurrence of X-ray flares at later times cannot be ruled out owing to low count rates). The H I creating the DLA is likely to be located much further away from the the GRB, unaffected by the GRB radiation. We would expect to observe destruction by the GRB of dust co-located with the X-ray absorbing gas. Our spectra imply a very low extinction in the host at ~ 3 hrs post burst. Future prompt optical spectra, in conjunction with X-ray observations, are required to investigate this further.

Acknowledgements. We thank P. A. Curran, A. J. van der Horst, K. L. Page and S. Vaughan for useful discussions. This work is based on observations made with the WHT operated on the island of La Palma by the Isaac Newton Group in the Spanish Observatorio del Roque de los Muchachos at the Instituto de Astrofísica de Canarias - we thank N. O'Mahony for excellent support. The authors acknowledge benefits from collaboration within the EU-funded Research Training Network 'Gamma-Ray Bursts: an enigma and a tool' (HPRN-CT-2002-00294).

References

Andersen, M. I., Hjorth, J., Pedersen, H., et al. 2000, A&A, 364, L54
 Berger, E., Cowie, L. L., Kulkarni, S. R., et al. 2003, ApJ, 588, 99
 Blustin, A., Holland, S. T., Cucchiara, A., et al. 2005, GCN Circ. 3717
 Bouchet, P., Lequeux, J., Maurice, E., et al. 1985, A&A, 149, 330
 Burrows, D. N., Romano, P., Falcone, A., et al. 2005, Science accepted, astro-ph/0506130
 Chen, H.-W., Thompson, I., Prochaska, J. X., et al. 2005, GCN Circ. 3709
 Cobb, B. E., & Bailyn, C. D., et al. 2005, GCN Circ. 3708
 Conselice, C. J., Vreeswijk, P. M., Fruchter, A. S., et al. 2005, ApJ preprint doi:10.1086/432829
 Dickey, J. M., & Lockman, F. J. 1990, ARA&A, 28, 215
 Ellison, S. L., Hall, P. B., Lira, P. 2005, AJ in press, astro-ph/0507418
 Erb, D. K., Shapley, A. E., Pettini, M., et al., in preparation
 Fynbo, J. P. U., Jakobsson, P., Møller, P., et al. 2003, A&A, 406, L63
 Garnett, D. R. 2002, ApJ, 581, 1019
 Grevesse, N., & Sauval, A. J. 1998, Space Sci Rev, 85, 161
 Grupe, D., Kennea, J. A., & Burrows, D. N. 2005, GCN Circ. 3714
 Haislip, J., Kirschbaum, J., Reichart, D., et al. 2005, GCN Circ. 3712
 Hjorth, J., Møller, P., Gorosabel, J., et al. 2003, ApJ, 597, 699
 Holland, S. T., Barthelmy, S., Burrows, D. N., et al. 2005, GCN Circ. 3704
 Holman, M., Garnavich, P., & Stanek, K. Z. 2005, GCN Circ. 3727
 Kewley, L. J., & Ellison, S. L., in preparation
 King, A., O'Brien, P. T., Goad, M. R., et al. 2005, ApJL accepted, astro-ph/0508126
 Kobulnicky, H. A., & Kewley, L. J. 2004, ApJ, 617, 240
 Kobulnicky, H. A., Willmer, C. N. A., Weiner, B. J., et al. 2003, ApJ, 599, 1006
 Lamareille, F., Mouhcine, M., Lewis, I., et al. 2004, MNRAS, 350, 396
 Møller, P., Fynbo, J. P. U., Hjorth, J., et al. 2002, A&A, 396, 21
 Murphy, M. T., & Liske, J. 2004, MNRAS, 345, L31
 Pei, Y. 1992, ApJ, 395, 130
 Prochaska, J. X., Chen, H.-W., Bloom, J. S., et al. 2005, GCN Circ. 3732
 Rol, E., Starling, R. L. C., Wiersema, K., et al. 2005, GCN Circ. 3710
 Schlegel, D. J., Finkbeiner, D. P., & Davis, M. 2004, ApJ, 500, 525

Table 1. Lines detected above 3σ in the first and second epoch WHT spectra.^a. Submitted as on-line table only.

λ	$W_{\text{obs}}(\text{I})$	$W_{\text{obs}}(\text{II})$	ID	z
4683.0 ^b			$\text{Ly}\beta \lambda 1025.722$	3.5656
5090.6 ^b			$\text{Ly}\beta \lambda 1025.722$	3.9629
5549.2 ^b			$\text{Ly}\alpha \lambda 1215.668$	3.5647
6031.5 ^b			$\text{Ly}\alpha \lambda 1215.668$	3.9615
6230.8	1.42 ± 0.24	1.19 ± 0.38	$\text{S II } \lambda 1253.805$	3.9695
6261.9	3.64 ± 0.25	3.50 ± 0.41	$\text{Si II } \lambda 1260.422$	3.9681
	blended with		$\text{S II } \lambda 1259.518$	3.9717
6283.9	3.95 ± 0.23	3.45 ± 0.33	$\text{Si II}^* \lambda 1264.738$	3.9685
6364.2	0.51 ± 0.17	0.78 ± 0.35	$\text{C I? } \lambda 1280.135$	3.9715
6470.8	1.95 ± 0.17	2.43 ± 0.39	$\text{O I } \lambda 1302.169$	3.9692
6482.8	2.57 ± 0.14	2.87 ± 0.28	$\text{O I}^* \lambda 1304.858$	3.9682
	blended with		$\text{Si II } \lambda 1304.370$	3.9700
6489.8	0.50 ± 0.11	0.82 ± 0.20	$\text{O I}^{**} \lambda 1306.029$	3.9691
6504.6	1.86 ± 0.16	2.17 ± 0.35	$\text{Si II}^* \lambda 1309.276$	3.9681
	blended with?		$\text{Fe II } \lambda 2344.214$	1.7747
6544.6	0.44 ± 0.13	0.47 ± 0.17		
6583.9	0.42 ± 0.10	0.55 ± 0.18		
6588.9	0.55 ± 0.11	0.57 ± 0.17		
6597.1	0.82 ± 0.12	1.33 ± 0.26		
6607.0	1.24 ± 0.14	1.58 ± 0.23	$\text{Fe II } \lambda 2382.765$	1.7728
6633.4	5.12 ± 0.19	5.07 ± 0.31	$\text{C II } \lambda 1334.532$	3.9706
	blended with		$\text{C II}^* \lambda 1335.663$	3.9664
6721.0	1.05 ± 0.17	0.73 ± 0.20		
6924.1	2.43 ± 0.15	2.42 ± 0.32	$\text{Si IV } \lambda 1393.760$	3.9679
6934.0	0.88 ± 0.09	1.18 ± 0.24		
6968.7	2.67 ± 0.15	2.32 ± 0.28	$\text{Si IV } \lambda 1402.773$	3.9678
	blended with		$\text{Si II } \lambda 1526.707$	3.5645
6989.4	1.44 ± 0.17	1.28 ± 0.22		
7000.9	0.52 ± 0.09	0.86 ± 0.24	$\text{Si II}^* \lambda 1533.432$	3.5655
7066.1	0.42 ± 0.12	0.20 ± 0.19	$\text{C IV } \lambda 1548.204$	3.5641
7077.7	0.32 ± 0.12	0.48 ± 0.18	$\text{C IV } \lambda 1550.781$	3.5640
7107.4	0.62 ± 0.14	0.61 ± 0.22		
7172.6	0.71 ± 0.14	0.92 ± 0.25	$\text{Fe II } \lambda 2586.650$	1.7729
7209.0	1.46 ± 0.17	0.86 ± 0.20	$\text{Fe II } \lambda 2600.173$	1.7725
7586.4 ^c	2.53 ± 0.18	2.48 ± 0.26	$\text{Si II } \lambda 1526.707$	3.9691
7628.5 ^c			$\text{Al II } \lambda 1670.789$	3.5658
7692.9	3.79 ± 0.14	3.86 ± 0.29	$\text{C IV } \lambda 1548.204$	3.9689
7705.3	3.66 ± 0.20	4.22 ± 0.36	$\text{C IV } \lambda 1550.781$	3.9687
7754.9	4.18 ± 0.34	5.15 ± 0.63	$\text{Mg II } \lambda 2798.743$	1.7709
7775.5	2.28 ± 0.25	2.67 ± 0.36	$\text{Mg II } \lambda 2803.532$	1.7735
7994.3	3.14 ± 0.54	3.27 ± 0.74	$\text{Fe II } \lambda 1608.451$	3.9716

^a Blueward of $\text{Ly}\alpha$ the low resolution and $\text{Ly}\alpha$ forest hampers secure identification of metal lines, which we therefore do not list.

^b Due to the uncertain continuum level, we do not attempt to measure the widths of the $\text{Ly}\alpha$ and $\text{Ly}\beta$ lines.

^c This equivalent width measurement is seriously affected or made impossible by the atmospheric absorption band from 7584–7675Å.

Shapley, A. E., Erb, D. K., Pettini, M., et al. 2004, ApJ, 612, 108
 Sota, A., Castro-Tirado, A. J., Guziy, S., et al. 2005, GCN Circ. 3705
 Tremonti, C., Heckman, T. M., Kauffmann, G., et al. 2004, ApJ, 613,
 898
 Vreeswijk, P. M., Ellison, S. L., Ledoux, C., et al. 2004, A&A, 419,
 927
 Wilms, J., Allen, A., & McCray, R. 2000, ApJ, 542, 914